

# Self-Assembled ZnO Nanoparticle Capsules for Carrying and Delivering Isotretinoin to Cancer Cells

Wei Zhao,<sup>†</sup> Ji-Shi Wei,<sup>†</sup> Peng Zhang,<sup>†</sup> Jie Chen,<sup>†</sup> Ji-Lie Kong,<sup>\*,†,‡</sup> Lian-Hua Sun,<sup>§</sup> Huan-Ming Xiong,<sup>\*,†,‡</sup> and Helmuth Möhwald<sup>||</sup>

<sup>†</sup>Department of Chemistry and Shanghai Key Laboratory of Molecular Catalysis and Innovative Materials, Fudan University, Shanghai 200433, P. R. China

<sup>‡</sup>Institutes of Biomedical Sciences, Fudan University, Shanghai 200032, P. R. China

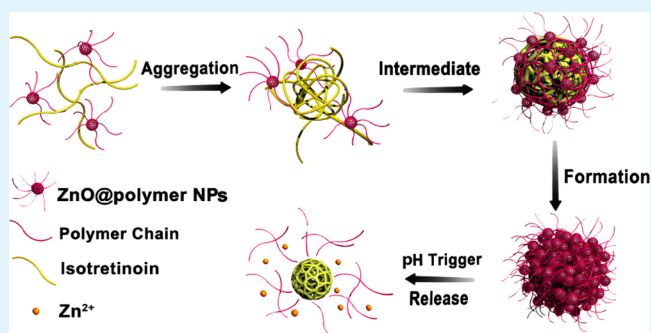
<sup>§</sup>Ear Institute, Shanghai Jiaotong University School of Medicine, Shanghai 200240, P. R. China

<sup>||</sup>Max-Planck Institute of Colloids and Interfaces, Potsdam 14424, Germany

## S Supporting Information

**ABSTRACT:** ZnO@polymer core–shell nanoparticles are assembled into novel capsule shells with diameters of about 100 nm to load isotretinoin (ISO) with a capacity as high as 34.6 wt %. Although ISO, a widely used drug for acne treatment, by itself is not suitable for treating cancer because of its hydrophobicity, our ZnO–ISO composite showed much stronger anticancer activity. The improved cytotoxicity is ascribed to the synergistic effects of the ZnO@polymer and ISO, where the ZnO@polymer helps in the accumulation of ISO in cancer cells on the one hand, and on the other hand, ISO is released completely through ZnO decomposition under acidic conditions of cancer cells. Such a pH-triggered drug-delivery system exhibits a much improved killing of cancer cells *in vitro* in comparison with the benchmarks, Nintedanib and Crizotinib, two commercial drugs clinically applied against lung cancer.

**KEYWORDS:** ZnO nanoparticle, isotretinoin, core–shell, drug delivery, cancer cell



## INTRODUCTION

Since the enhanced permeability and retention (EPR) effect of nanomaterials in solid tumors was recognized,<sup>1,2</sup> numerous nanoparticles (NPs) have been synthesized and used to carry anticancer drugs for chemotherapy, including rare earth NPs,<sup>3,4</sup> metal oxide NPs,<sup>5,6</sup> Au NPs,<sup>7,8</sup> carbon NPs,<sup>9,10</sup> silica NPs,<sup>11,12</sup> and polymer NPs.<sup>13,14</sup> Although these drug-delivery systems (DDSs) based on NPs have shown promising therapeutic efficacy, there are four main limitations to be overcome. One is that most NPs are neither biodegradable nor metabolic for animals, which provide unexpected potential toxicity chronically. The second is the competition between carrier stability and drug delivery: For a very stable DDS in the circulatory system, the drugs should be enclosed tightly, so that both the loading efficiency and the release rate of the drugs are low. The third is the response mechanism for drug delivery: Many novel response conditions, like light irradiation,<sup>15–17</sup> ultrasound vibration,<sup>18,19</sup> and magnetic field,<sup>20–22</sup> are based on complicated structures and multistep preparations, which cause nonuniformity of the DDSs and more difficulties in biodegradation and metabolism. Last but not least, the DDS should have good dispersibility and long-term stability in water, which is a real challenge, because many drugs are hydrophobic and most NPs are apt to agglomerate during storage.

ZnO NPs are expected to overcome the above limitations after suitable design and controlled synthesis.<sup>23</sup> They have gained many practical applications in biomedical areas due to their low cost, high stability, and production safety. We have also proved their stability and safety in bioimaging,<sup>24,25</sup> protein enrichment,<sup>26</sup> and drug delivery.<sup>27</sup> Recently, we found that ZnO@polymer core–shell NPs decomposed completely under the acidic environment of cancer cells; we used them to carry doxorubicin (DOX) to treat mouse tumors effectively without any toxic side effects.<sup>28</sup> However, the stable loading capacity of DOX was only 17.2 wt %, because more drug on the ZnO surface would be washed off in a buffer solution. For a higher loading capacity with long-term stability, new structures of ZnO-based DDSs should be realized.

Isotretinoin (ISO) is a popular medicine for acne treatment.<sup>29–31</sup> It is also a potential anticancer drug designed to combine with those specific receptors in cancer cells, so as to improve the efficacy and avoid unwanted side effects,<sup>32,33</sup> but its anticancer ability is insufficient due to insolubility in water. Because of this limitation, and the fact that many other

Received: February 21, 2017

Accepted: May 17, 2017

Published: May 25, 2017

hydrophobic drugs fail due to their poor bioavailability,<sup>34</sup> previous works utilized solid lipid nanoparticles<sup>35,36</sup> or nanostructured lipid carriers<sup>37,38</sup> to carry ISO. Unfortunately, the thick shell of the lipids often hindered the high load and the complete release of ISO. Until now, there has been no successful report on the coating and carrying of ISO by NPs for anticancer studies. In the present research, we found that ZnO@polymer NPs and ISO can self-assemble to a new composite, ZnO–ISO, in which ZnO@polymer NPs were surrounding a million ISO molecules to form monodisperse spheres with diameters of about 100 nm. Such capsules with a ZnO@polymer NP shell were able to contain ISO as high as 34.6 wt % and remained stable in neutral solutions for more than 1 year, just like the pre-eminent organic–inorganic self-assembled NPs for cancer therapy.<sup>39–42</sup> Distinguished from those lipid-constructed micelles, ZnO@polymer NPs decompose in the acidic environment of the tumor cells and release ISO completely to kill the cancer cells. After optimization, our ZnO–ISO composite showed much stronger anticancer ability than pure ISO and even exceeded two commercial drugs Nintedanib and Crizotinib, which are applied clinically against lung cancer.

## EXPERIMENTAL SECTION

**Synthesis and Characterization.** ISO (0.025 g) was dissolved in 25 mL of dimethyl sulfoxide (DMSO) and stored in the dark (solution A). ZnO@polymer NPs were synthesized according to our previous method.<sup>43</sup> Briefly, zinc methacrylate was obtained by a reaction between ZnO powder and methacrylic acid aqueous solution. In absolute ethanol, dried zinc methacrylate, poly(ethylene glycol) methyl ether methacrylate (PEGMEMA, average  $M_n = 500$ ) monomers and 2'-azobis(isobutyronitrile) (AIBN) were added and dissolved at 72 °C. After prepolymerization for 15 min, appropriate amounts of LiOH ethanol solution and another dose of AIBN were added and then the reaction mixture was refluxed for 1 h. The obtained clear solution was dialyzed against water for 3 days to remove ethanol and any other ions or molecules. This as-prepared aqueous solution B was measured by ICP and weighed to determine the weight concentration of ZnO@polymer NPs. An appropriate amount of solution A was added into 10 mL of solution B and stirred in the dark for 12 h. Then, the solution was dialyzed for 3 days against deionized water. The UV–vis absorption data were recorded by a Unico 2802 UV–vis spectrometer. Transmission electron microscope (TEM) images were obtained using a JEM-2010 TEM operating at 200 kV. Field emission scanning electron microscopy (FESEM) was measured by a Hitachi S4800 scanning electron microscope. The dynamic light scattering (DLS) spectra and zeta potentials were measured by a Malvern ZS-90 Zetasizer. The relaxation time of the samples was measured by a MiniPQ001-20-015V low field nuclear magnetic resonance spectrometer. Fourier transform infrared (FTIR) spectra were recorded on a Nicolet iS10 FTIR spectrometer in a range of 4000–400  $\text{cm}^{-1}$ , using the KBr pellet method.

**Drug Release.** To study ISO release in acetate buffer solution, 30 mg of ZnO–ISO NPs was dissolved in 3 mL of three buffer solutions (pH 5.0, 6.0, and 7.0), respectively. Then, it was sealed in a dialysis bag (molecular weight cutoff of 8000) and dialyzed against 20 mL of the corresponding buffer solution. During dialysis for 2 days, the outside buffer solution was replaced by 20 mL of a new buffer solution at different time intervals. The released ISO in the buffer solutions was collected, and its concentration was analyzed by UV–vis spectroscopy according to its typical absorption at 399 nm.

**MTT Assay.** All cell culture processes in this work were carried out with 5%  $\text{CO}_2$  at 37 °C. A549, Hela, DU145, and MCF-7 cells were all seeded at  $5 \times 10^3$  cells per well into a 96-well cell culture plate in Dulbecco's modified Eagle medium (DMEM) with 10% fetal bovine serum (FBS) for 24 h. Then, the culture medium was replaced by the culture medium containing drugs with various concentrations for

another 24 h. Afterward, cells were incubated with 100  $\mu\text{L}$  of the new culture medium and 20  $\mu\text{L}$  of MTT (thiazolyl blue tetrazolium bromide, 5 mg/mL in phosphate-buffered saline (PBS)) for 4 h. After the medium was removed, formazan crystals were dissolved with DMSO for 10 min, and the absorbance of MTT at 492 nm was measured by an automatic scanning multiwall spectrometer (SPR-960; Sunostik).

**Fluorescence Activated Cell Sorting.** First, A549 cells were cultivated in DMEM with 10% FBS for 24 h and then they were treated with 1, 2, 4, 8, and 16  $\mu\text{g}/\text{mL}$  ZnO–ISO for another 48 h. Afterward, the cells were collected and floated in PBS for washing and then incubated at a concentration of  $2 \times 10^6$  cells/mL with Annexin V-FITC and PI for 15 min and finally analyzed by a Beckman Gallios flow cytometer. In the dot plots, the cells in the lower left were viable and negative for both annexin V and PI, the early apoptotic cells in the lower right were positive for annexin V but negative for PI, the late apoptotic cells in the upper right were positive for annexin V and PI, and the necrotic cells in the upper left were positive for PI but negative for annexin V.

**Cell Imaging.** The hydrophobic NIR fluorescent dye, IR780, was modified on the ZnO–ISO NPs for tracking the uptake of the drug. The obtained ZnO–ISO–IR780 was incubated with A549 cells for 2, 6, and 24 h, respectively, with an ISO concentration of 10  $\mu\text{g}/\text{mL}$ . An Olympus FV1000 confocal laser scanning microscope (CLSM) was used to observe the cells.

## RESULTS AND DISCUSSION

The ZnO@polymer core–shell NPs were synthesized and dispersed in water, whereas ISO was dissolved in DMSO before use. Although ISO is insoluble in water, when the above two solutions were mixed in appropriate ratios, a series of stable transparent solutions were obtained, which remained stable even after DMSO removal through dialysis. Such a ZnO–ISO solution turned turbid, when the pH value was tuned below 6, indicating ZnO decomposition and drug release (Scheme 1).

### Scheme 1. Formation and Decomposition of ZnO–ISO

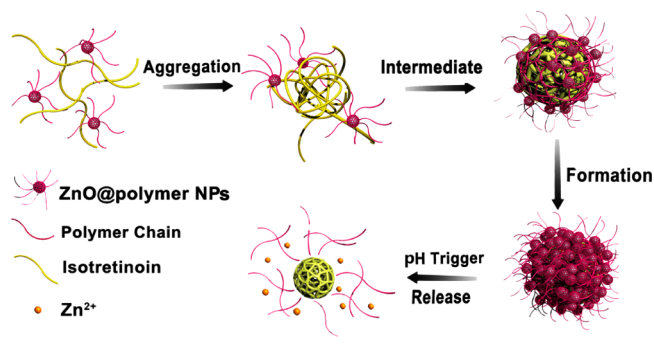
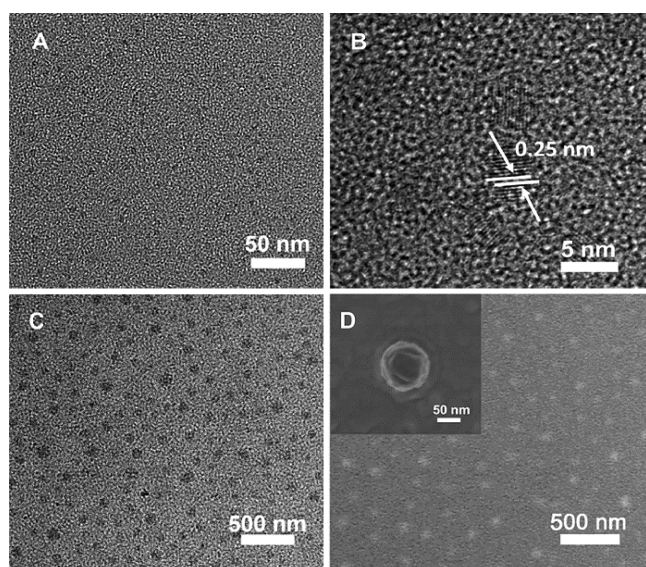


Figure 1A,B shows that the ZnO@polymer core–shell NPs are uniform and monodisperse in water, with an average diameter of 3 nm and a lattice spacing of 0.25 nm, corresponding to the wurzite structure. The TEM image (Figure 1C) shows that ISO forms monodisperse spheres of about 100 nm, with ZnO NPs attached on the surfaces. The SEM image at low magnification (Figure 1D) also confirms the good dispersity and the uniform particle size of ZnO–ISO, whereas the SEM image at high magnification (Figure 1D, inset) clearly shows that ZnO–ISO has a core–shell structure in which ZnO@polymer NPs are covering the ISO sphere.

When the ZnO@polymer and ISO were mixed in mass ratios higher than 1:0.5, the products, ZnO–ISO, were stable in water. More ISO addition yielded a turbid solution. The average particle diameter of ZnO–ISO increased from about 80



**Figure 1.** (A) TEM image and (B) HRTEM image of ZnO NPs. (C) TEM image and (D) low-magnification SEM image with the inset high-magnification SEM image of the ZnO–ISO composites (the weight ratio for the preparation is 1:0.5).

to 110 nm, as the mass ratio was increased from 1:0.1 to 1:0.5 (Figures S1, S2, and S4). Both the TEM images and DLS data confirmed the uniformity of our DDS. We chose the ratio of 1:0.5 as the optimal ratio, because the as-prepared ZnO–ISO had the highest content of ISO. By optical analyses and ICP measurements, the highest loading content of ISO was determined to be 34.6 wt % for the optimal ZnO–ISO ratio, much higher than that for many other DDSs. In this sample, the polymer and ZnO contents were found to be 59.3 and 6.1 wt %, respectively. If we assume the ISO spheres to be solid with a diameter of 100 nm, each ZnO–ISO particle would contain about  $1.05 \times 10^6$  ISO molecules, which would be surrounded by about 1170 ZnO NPs. This amounts to a surface density of 1 NP/27 nm<sup>2</sup>. However, our calculation shows that the cross-section area of the ZnO@polymer NP is larger than 100 nm<sup>2</sup>. This indicates that either the ISO sphere is not simply coated by a single layer of the ZnO shell like that in Scheme 1 or the ISO particle is porous with a rough surface. We tend to assume the first case, because even the SEM image in Figure 1D indicates a thicker shell around an ISO sphere. The zeta potential of this sample in water was measured to be  $-28.2$  mV,

also confirming the stability of ZnO–ISO. After 1 year of storage, our sample is still stable (Figure S6).

ZnO@polymer NPs possess bright green fluorescence under UV light, but ZnO–ISO nanocomposites are not luminescent. To study this issue, the UV–vis spectra of ISO, ZnO–ISO, and ZnO NP solutions are compared in Figure 2A. ISO shows a strong absorption peak at 370 nm, corresponding to its conjugated polyene structure, whereas ZnO exhibits its bandgap absorption band at about 330 nm. For ZnO–ISO, the absorption at 330 nm becomes stronger due to the overlap of the absorption of both ZnO and ISO, which proves that ZnO NPs are not destroyed by ISO. Therefore, the ZnO fluorescence quenching in ZnO–ISO is ascribed to the energy transfer from ZnO to nonfluorescent ISO. Strong interactions are also illustrated by shifts in the FTIR spectra (Figure 2B). The ISO molecule has a COOH group on its end and five conjugated double bonds in its chain. The C=O vibration at 1653 cm<sup>-1</sup> and the C–O vibration at 1430 cm<sup>-1</sup> are therefore ascribed to the COOH groups of ISO. For the ZnO@polymer, the FTIR bands at 1718 and 1612 cm<sup>-1</sup> are due to the coordination between carboxyl groups of the polymers and ZnO NPs, and the C–O–C vibration at 1100 cm<sup>-1</sup> is from the polymer chains. In ZnO–ISO, the vibrations at 1720, 1617, and 1456 cm<sup>-1</sup> become much stronger, indicating that new coordination bonds have formed between the Zn atoms from ZnO and the COOH groups from ISO through a bridging mode.<sup>44</sup>

It is well known that tumor cells provide an acidic environment, especially in the lysosomes and the endosomes. We have previously utilized this feature to decompose ZnO NPs to release DOX, but the drug loaded on ZnO NP surfaces was quickly lost, and the loading capacity was limited by the surface areas. However, in the present research, many ZnO NPs form a small capsule shell containing the aggregated ISO molecules, which is much more stable due to the hydrophilic–hydrophobic interactions. Figure 3A shows that almost no ISO leaked out after the initial 4 h dialysis. The initially lost ISO molecules were probably those adsorbed on the ZnO–ISO surfaces. Furthermore, such a ZnO–ISO structure is more sensitive than drug-coated ZnO NPs, because ZnO NPs are exposed toward the outside solution. When the pH value decreases below 6, ZnO–ISO decomposes quickly, and more than 90% of the drug is released within 8 h. To further study the state of this DDS at different pH values, we used low-field nuclear magnetic resonance to evaluate the relative hydrophobicity of ZnO–ISO, which is reflected in the relaxation time. Figure 3B shows that distilled water has a relaxation time

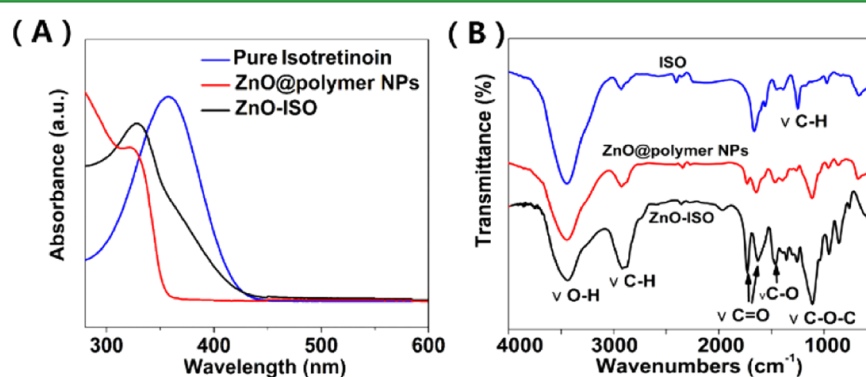


**Figure 2.** (A) UV–vis absorption and (B) FTIR spectra of ISO, ZnO@polymer NPs, and ZnO–ISO composites.

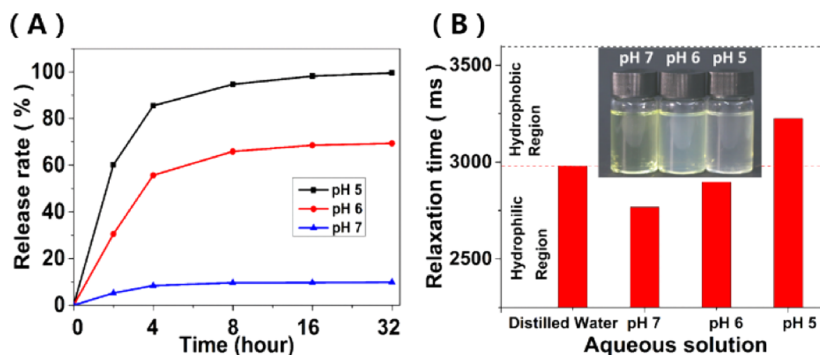


**Figure 3.** (A) Released amount of ISO from ZnO–ISO at different pH values. (B) Relaxation time measured by low-field nuclear magnetic resonance for ZnO–ISO solutions at different pH values, with distilled water as the control. The inset photo shows that the solution turns turbid if the pH value is decreased.

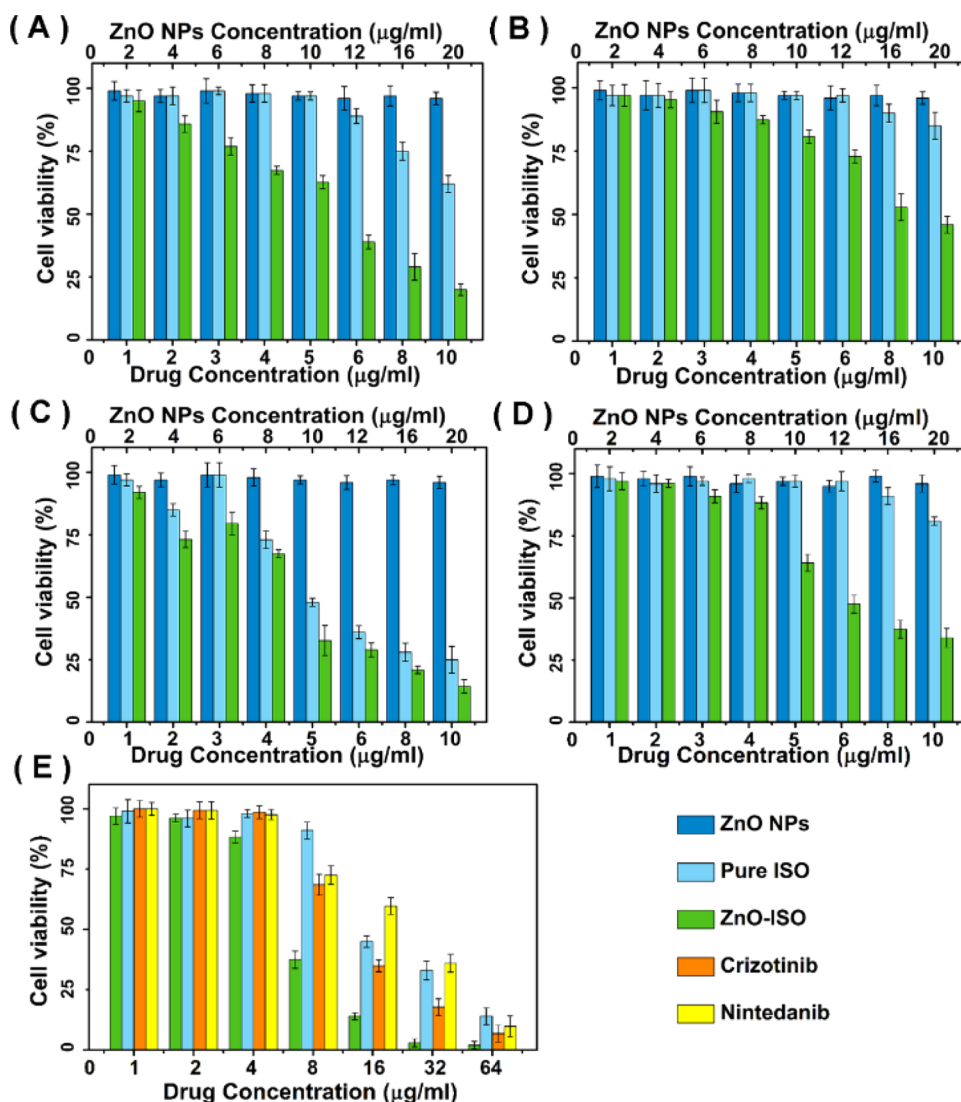


**Figure 4.** Cytotoxicity of ZnO NP, pure ISO, and ZnO–ISO toward tumor cells (A) DU145, (B) HeLa, (C) MCF-7, and (D) A549, respectively, from MTT assays. (E) Cytotoxicity toward lung cancer cells A549 of ZnO–ISO, ISO, Crizotinib, and Nintedanib at different concentrations, respectively.

of 2900 ms, which is regarded as a boundary between the hydrophilic and the hydrophobic regions. It is obvious that ZnO–ISO is stable at pH 7 but unstable at pH 6. When the pH value decreases to 5, the relaxation time of the species in water increases to 3225 ms, which means that a lot of hydrophobic

ISO molecules have been released. Although the ZnO content in ZnO–ISO is small, it plays a key role because the polymer cannot keep ISO stable in water after ZnO decomposition.

Retinoic acids as natural derivatives of vitamin A play important roles in cell differentiation, growth, and apoptosis.

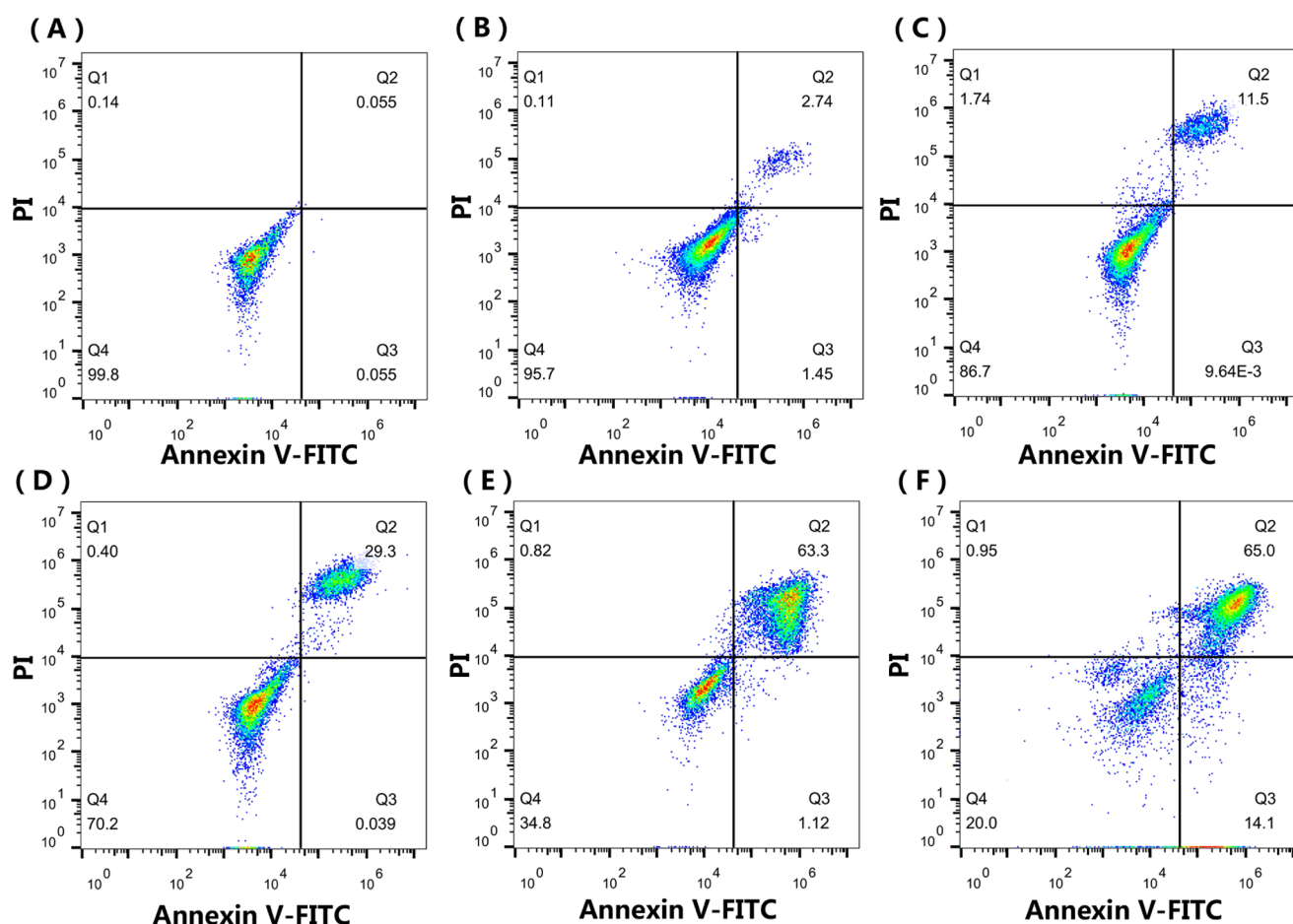


**Figure 5.** Flow cytometry data for A549 cells after incubation with (A) 0, (B) 1  $\mu\text{g/mL}$ , (C) 2  $\mu\text{g/mL}$ , (D) 4  $\mu\text{g/mL}$ , (E) 8  $\mu\text{g/mL}$ , and (F) 16  $\mu\text{g/mL}$  of ZnO–ISO for 48 h, respectively. The cells are stained with Annexin V-FITC and PI. Dot plots of FITC-labeled Annexin V (horizontal axis) and PI fluorescence (vertical axis) are shown with the logarithmic fluorescence intensity. Quadrants: lower left, live cells; lower right, early apoptotic cells; upper right, late apoptotic cells; upper left, dead (necrotic) cells.

ISO is one of the metabolized products from retinoic acids, which exhibits special immunomodulatory and anti-inflammatory responses. However, anticancer effects of ISO toward many cancers are poor, probably due to its insolubility in water.<sup>45</sup> In the present work, we tested the cytotoxicity of pure ISO and ZnO–ISO by MTT assays toward several kinds of cancer cells (Figure 4). A DMSO solution of ISO was diluted by a large volume of water (DMSO/water = 1:1000) to obtain a clear solution for cell incubation. Different cells were incubated with drugs for 12, 24, and 48 h (Figure S7). After incubation, the 48 h MTT results were similar to the 24 h MTT results, so we used the data of 24 h incubation for further analyses (Table S2). Although the pure ISO was almost nontoxic for tumor cells except MCF-7, cytotoxicity of ZnO–ISO was strong for all cells tested. If the concentration of ISO in ZnO–ISO is above 8  $\mu\text{g/mL}$ , most of the cancer cells are killed after 24 h of incubation. The enhanced cytotoxicity of ZnO–ISO cannot be ascribed to ZnO NPs, because the  $\text{IC}_{50}$  for our ZnO NPs toward cancer cells is typically about 200  $\mu\text{g/mL}$ .<sup>43,46</sup> Therefore, the enhanced cytotoxicity is based on the ZnO carriers that overcome the hydrophobicity of ISO and accumulate high concentrations of ISO in the cells.

After a general investigation of the anticancer effects of ZnO–ISO, a deep insight into cytotoxicity was obtained by studies of A549, a kind of nonsmall cell lung cancer cell. To compare ZnO–ISO with the two commercial lung cancer

drugs, Nintedanib<sup>47</sup> and Crizotinib,<sup>48</sup> we also loaded Nintedanib and Crizotinib onto ZnO@polymer NPs by the same method (Table S1). The UV–vis absorption spectra confirm the successful loading (Figure S8). TEM results show that both ZnO–Nintedanib and ZnO–Crizotinib are monodisperse NPs (Figure S9), with diameters of about 5 nm. Unlike ISO, both Nintedanib and Crizotinib are soluble in water, so they are just adsorbed on the ZnO surfaces to form ZnO–Nintedanib and ZnO–Crizotinib, respectively, similar to the ZnO–DOX in our previous reports.<sup>27,28</sup> Owing to such a difference in structure (Scheme S1), the loaded amounts of both Nintedanib and Crizotinib on ZnO NPs are only 7.4 and 6.9 wt %, respectively. Because the ZnO contents in these two DDSs are significantly higher than those in ZnO–ISO, the toxicity of ZnO NPs cannot be ignored in the MTT assays. Figure S10 shows that at high concentrations, the toxicities of both ZnO–Nintedanib and ZnO–Crizotinib are a little higher than those of Nintedanib and Crizotinib, respectively. Such differences can be ascribed to the ZnO toxicity, but the main anticancer effects are still from Nintedanib and Crizotinib. To study the cytotoxicity of ZnO–ISO over a wide range, we incubated A549 cells with higher concentrations of ZnO–ISO, as well as the three drugs. The results in Figure 4 clearly show that the toxicity of ZnO–ISO toward A549 is much higher than that of the three drugs. When the ISO concentration is above 4  $\mu\text{g/mL}$ , ZnO–ISO begins to exhibit strong cytotoxicity. It

should be mentioned that our MTT results of ISO, Nintedanib, and Crizotinib are consistent with those previous reports.<sup>49–51</sup>

To understand the anticancer activity and mechanism of ZnO–ISO, we used PI and Annexin V-FITC to stain A549 cells and monitored by flow cytometry the procedures after the cells were pretreated by different concentrations of ZnO–ISO. All ISO concentrations were kept consistent with those in the above MTT experiments; however, the incubation time was extended to 48 h. Figure 5A shows that after the untreated A549 cells have grown naturally with high viability, almost all cells are both Annexin V and PI negative. But after incubation with ZnO–ISO, the situations of the cells change significantly. More and more cells turn into late apoptosis or death as the ZnO–ISO concentration is gradually increased, and only 16  $\mu\text{g}/\text{mL}$  ISO in the ZnO–ISO composites is able to convert more than 80% of A549 cells into apoptosis. These results confirm that cell apoptosis has been induced by ISO, and this process might be ascribed to genetic mutation triggered by the ISO transported into the nucleus.

To further analyze the drug-release process of the ZnO–ISO nanocapsules, we loaded the hydrophobic fluorescent dye, IR780, onto ZnO–ISO for tracking the intracellular pathway and intracellular location of ZnO–ISO by CLSM techniques. DAPI was used to indicate the position of the nucleus; it was incubated with the cells together with the ZnO–ISO–IR780. In Figure 6, after 2 h of incubation, only a little amount of the

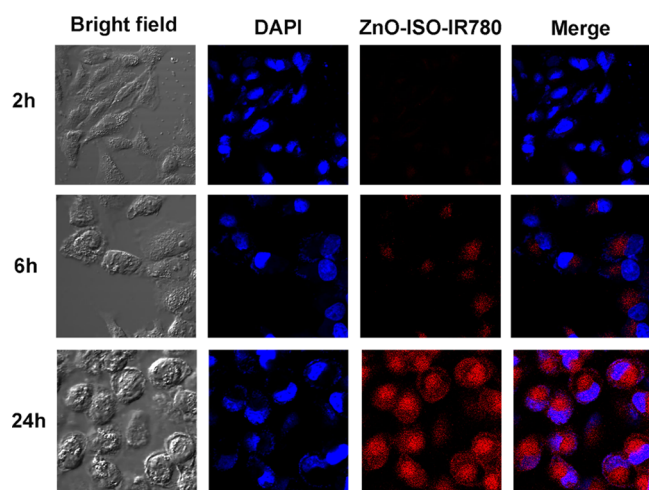
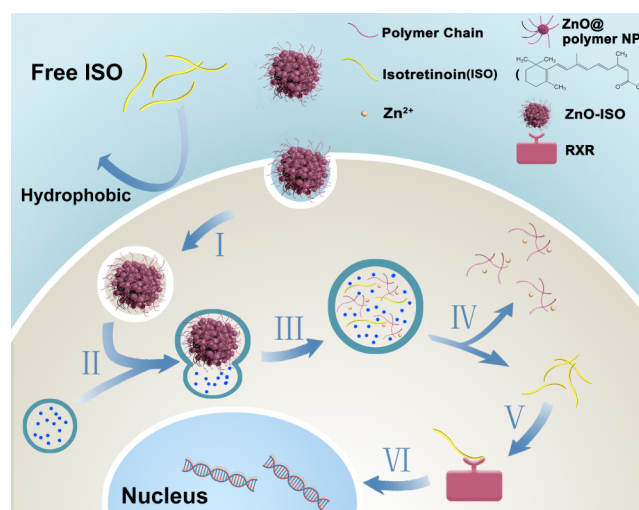


**Figure 6.** CLSM images of A549 cells treated with DAPI (blue) and ZnO–ISO–IR780 (red) for 2, 6, and 24 h, respectively. These images were taken by a 63 times objective lens.

drug entered the A549 cells, and the cells had normal morphologies. After 6 h of incubation, more amount of the drug was uptaken, the red fluorescence of IR780 was seen in the cells, and the morphologies of the cells showed that they were in the state of early apoptosis. After 24 h of incubation, a significant amount of the drug was uptaken by the cells, and most cells curled up and died. Finally, the IR780 was located at both the cytoplasm and the nucleus.

The above results verify that the anticancer ability of ZnO–ISO is much stronger than that of both pure ISO and sole ZnO@polymer NPs. To illustrate this synergistic effect, we suppose that ZnO–ISO nanocomposites are uptaken by the cells and then engulfed by lysosomes (Scheme 2). Unlike pure ISO, ZnO–ISO has an affinity for both the cell membrane and the cell sap, so they can easily enter the cell and accumulate to a

## Scheme 2. Proposed Mechanism for ISO Delivery into A549 Cells<sup>a</sup>



<sup>a</sup>In contrast to free ISO, ZnO–ISO NPs can penetrate the cell membrane (I), be uptaken by lysosomes (II), where the ZnO shells are destroyed (III), releasing the drug and the polymer (IV). It is then taken up by specific receptors (V) and transported to the nucleus (VI).

high concentration. It has been reported that retinoic acids exert their functions through their special receptors, such as retinoic acid receptors and retinoic X receptors (RXR).<sup>52,53</sup> For ISO, the receptors were named RXR.<sup>54</sup> ISO–RXR heterodimers activate themselves to the target genes in the nucleus and then have downstream gene expression. This signal pathway can finally trigger cell apoptosis.<sup>55</sup> In brief, the acidic environment of lysosomes decomposes ZnO capsules to release ISO molecules, which promotes the apoptosis genes to induce cell death.

## CONCLUSIONS

Stable aqueous ZnO@polymer core–shell NPs were synthesized for loading drugs to kill cancer cells. Two commercial anticancer drugs, Nintedanib and Crizotinib, and one commercial acne drug, ISO, were studied and compared in this work. Several kinds of cancer cells were used for the MTT assays, and A549 cells were further investigated by flow cytometry and CLSM to disclose the mechanism. ZnO–ISO showed a much better anticancer effect than both Nintedanib and Crizotinib within a wide range of drug concentrations; these results are exciting and promising. Its anticancer ability of ZnO–ISO is also stronger than that of both pure ISO and sole ZnO NPs. Such a synergistic effect is based on the unique structure of our DDS, in which ZnO@polymer NPs self-assemble into capsule shells to load ISO. This novel capsule structure has three advantages over the simple NP–drug surface loading mode. First, the drugs do not leak and flow out, because they are packaged tightly inside and possess low water solubility. Second, the loading capacity of the capsules is evidently higher than that on NP surfaces. Finally, the pH sensitivity of ZnO–ISO is also higher because ZnO NPs are located outside the ISO spheres. Our present research confirms that ZnO@polymer NPs are most suitable for carrying hydrophobic drugs to treat tumors. It may become a general procedure to assemble more hydrophobic drugs with superior anticancer efficiency as NPs with a pH-sensitive shell, a good dispersibility in water, and a controlled release on demand.

## ■ ASSOCIATED CONTENT

## S Supporting Information

The Supporting Information is available free of charge on the ACS Publications website at DOI: 10.1021/acsami.7b02542.

DLS data, TEM images, UV-vis absorption spectra, cell viabilities, and some discussion (PDF)

## ■ AUTHOR INFORMATION

## Corresponding Authors

\*E-mail: jlkong@fudan.edu.cn (J.-L.K.).

\*E-mail: hmxiong@fudan.edu.cn (H.-M.X.).

ORCID 

Huan-Ming Xiong: 0000-0002-3118-942X

## Notes

The authors declare no competing financial interest.

## ■ ACKNOWLEDGMENTS

This work was supported by National Major Basic Research Program of China (2013CB934101), the National Natural Science Foundation of China (21271045, 21335002, 21427806, 11074053, and 31170802), the Shanghai Leading Academic Discipline Project (B109), and the Shanghai Science and Technology Committee (16DZ2270100).

## ■ REFERENCES

(1) Maeda, H.; Wu, J.; Sawa, T.; Matsumura, Y.; Hori, K. Tumor Vascular Permeability and the EPR Effect in Macromolecular Therapeutics: a Review. *J. Controlled Release* **2000**, *65*, 271–284.

(2) Maeda, H. the Enhanced Permeability and Retention (EPR) Effect in Tumor Vasculature: the Key Role of Tumor-Selective Macromolecular Drug Targeting. *Adv. Enzyme Regul.* **2001**, *41*, 189–207.

(3) Xiao, Q.; Zheng, X.; Bu, W.; Ge, W.; Zhang, S.; Chen, F.; Xing, H.; Ren, Q.; Fan, W.; Zhao, K.; Hua, Y.; Shi, J. A Core/Satellite Multifunctional Nanotheranostic for *in Vivo* Imaging and Tumor Eradication by Radiation/Photothermal Synergistic Therapy. *J. Am. Chem. Soc.* **2013**, *135*, 13041–13048.

(4) Liu, Q.; Chen, M.; Sun, Y.; Chen, G.; Yang, T.; Gao, Y.; Zhang, X.; Li, F. Multifunctional Rare-Earth Self-Assembled Nanosystem for Tri-Modal Upconversion Luminescence/Fluorescence/Positron Emission Tomography Imaging. *Biomaterials* **2011**, *32*, 8243–8253.

(5) Wang, C.; Xu, H.; Liang, C.; Liu, Y.; Li, Z.; Yang, G.; Cheng, L.; Li, Y.; Liu, Z. Iron Oxide@Polypyrrole Nanoparticles as a Multifunctional Drug Carrier for Remotely Controlled Cancer Therapy with Synergistic Antitumor Effect. *ACS Nano* **2013**, *7*, 6782–6795.

(6) Tian, Y.; Jiang, X.; Chen, X.; Shao, Z.; Yang, W. Doxorubicin-Loaded Magnetic Silk Fibroin Nanoparticles for Targeted Therapy of Multidrug-Resistant Cancer. *Adv. Mater.* **2014**, *26*, 7393–7398.

(7) Shi, J.; Chen, Z.; Wang, L.; Wang, B.; Xu, L.; Hou, L.; Zhang, Z. A Tumor-Specific Cleavable Nanosystem of PEG-Modified C60@Au Hybrid Aggregates for Radio Frequency-Controlled Release, Hyperthermia, Photodynamic Therapy and X-Ray Imaging. *Acta Biomater.* **2016**, *29*, 282–297.

(8) Agarwal, A.; Mackey, M. A.; El-Sayed, M. A.; Bellamkonda, R. V. Remote Triggered Release of Doxorubicin in Tumors by Synergistic Application of Thermosensitive Liposomes and Gold Nanorods. *ACS Nano* **2011**, *5*, 4919–4926.

(9) Liu, Z.; Fan, A. C.; Rakhra, K.; Sherlock, S.; Goodwin, A.; Chen, X.; Yang, Q.; Felsher, D. W.; Dai, H. Supramolecular Stacking of Doxorubicin on Carbon Nanotubes for *in Vivo* Cancer Therapy. *Angew. Chem., Int. Ed.* **2009**, *48*, 7668–7672.

(10) Tang, J.; Kong, B.; Wu, H.; Xu, M.; Wang, Y.; Wang, Y.; Zhao, D.; Zheng, G. Carbon Nanodots Featuring Efficient FRET for Real-Time Monitoring of Drug Delivery and Two-Photon Imaging. *Adv. Mater.* **2013**, *25*, 6569–6574.

(11) Zhang, Q.; Liu, F.; Nguyen, K. T.; Ma, X.; Wang, X.; Xing, B.; Zhao, Y. Multifunctional Mesoporous Silica Nanoparticles for Cancer-Targeted and Controlled Drug Delivery. *Adv. Funct. Mater.* **2012**, *22*, 5144–5156.

(12) Argyo, C.; Weiss, V.; Bräuchle, C.; Bein, T. Multifunctional Mesoporous Silica Nanoparticles as a Universal Platform for Drug Delivery. *Chem. Mater.* **2014**, *26*, 435–451.

(13) Feng, L.; Yang, X.; Shi, X.; Tan, X.; Peng, R.; Wang, J.; Liu, Z. Polyethylene Glycol and Polyethyleneimine Dual-Functionalized Nano-Graphene Oxide for Photothermally Enhanced Gene Delivery. *Small* **2013**, *9*, 1989–1997.

(14) Topete, A.; Alatorre-Meda, M.; Iglesias, P.; Villar-Alvarez, E. M.; Barbosa, S.; Costoya, J. A.; Taboada, P.; Mosquera, V. Fluorescent Drug-Loaded, Polymeric-Based, Branched Gold Nanoshells for Localized Multimodal Therapy and Imaging of Tumoral Cells. *ACS Nano* **2014**, *8*, 2725–2738.

(15) Cui, S.; Yin, D.; Chen, Y.; Di, Y.; Chen, H.; Ma, Y.; Achilefu, S.; Gu, Y. In Vivo Targeted Deep-Tissue Photodynamic Therapy Based on Near-Infrared Light Triggered Upconversion Nanoconstruct. *ACS Nano* **2013**, *7*, 676–688.

(16) You, J.; Zhang, G.; Li, C. Exceptionally High Payload of Doxorubicin in Hollow Gold Nanospheres for Near-Infrared Light-Triggered Drug Release. *ACS Nano* **2010**, *4*, 1033–1041.

(17) Yuan, Q.; Zhang, Y.; Chen, T.; Lu, D.; Zhao, Z.; Zhang, X.; Li, Z.; Yan, C. H.; Tan, W. Photon-Manipulated Drug Release from a Mesoporous Nanocontainer Controlled by Azobenzene-Modified Nucleic Acid. *ACS Nano* **2012**, *6*, 6337–6344.

(18) Rapoport, N. Y.; Kennedy, A. M.; Shea, J. E.; Scaife, C. L.; Nam, K. H. Controlled and Targeted Tumor Chemotherapy by Ultrasound-Activated Nanoemulsions/Microbubbles. *J. Controlled Release* **2009**, *138*, 268–276.

(19) Schroeder, A.; Honen, R.; Turjeman, K.; Gabizon, A.; Kost, J.; Barenholz, Y. Ultrasound Triggered Release of Cisplatin from Liposomes in Murine Tumors. *J. Controlled Release* **2009**, *137*, 63–68.

(20) Cai, K.; Luo, Z.; Hu, Y.; Chen, X.; Liao, Y.; Yang, L.; Deng, L. Magnetically Triggered Reversible Controlled Drug Delivery from Microfabricated Polymeric Multireservoir Devices. *Adv. Mater.* **2009**, *21*, 4045–4049.

(21) Arias, J. L.; Reddy, L. H.; Othman, M.; Gillet, B.; Desmaële, D.; Zouhri, F.; Dosio, F.; Gref, R.; Couvreur, P. Squalene Based Nanocomposites: A New Platform for the Design of Multifunctional Pharmaceutical Theragnostics. *ACS Nano* **2011**, *5*, 1513–1521.

(22) Katagiri, K.; Imai, Y.; Koumoto, K.; Kaiden, T.; Kono, K.; Aoshima, S. Magneto-responsive On-Demand Release of Hybrid Liposomes Formed from Fe<sub>3</sub>O<sub>4</sub> Nanoparticles and Thermosensitive Block Copolymers. *Small* **2011**, *7*, 1683–1689.

(23) Xiong, H. M. ZnO Nanoparticles Applied to Bioimaging and Drug Delivery. *Adv. Mater.* **2013**, *25*, 5329–5335.

(24) Ma, Y. Y.; Ding, H.; Xiong, H. M. Folic Acid Functionalized ZnO Quantum Dots for Targeted Cancer Cell Imaging. *Nanotechnology* **2015**, *26*, 305702–305709.

(25) Zhang, H. J.; Xiong, H. M.; Ren, Q. G.; Xia, Y. Y.; Kong, J. L. ZnO@Silica Core-Shell Nanoparticles with Remarkable Luminescence and Stability in Cell Imaging. *J. Mater. Chem.* **2012**, *22*, 13159–13165.

(26) Shen, W. W.; Xiong, H. M.; Xu, Y.; Cai, S. J.; Lu, H. J.; Yang, P. Y. ZnO-Poly(Methyl Methacrylate) Nanobeads for Enriching and Desalting Low-Abundant Proteins Followed by Directly MALDI-TOF MS Analysis. *Anal. Chem.* **2008**, *80*, 6758–6763.

(27) Zhang, Z. Y.; Xu, Y. D.; Ma, Y. Y.; Qiu, L. L.; Wang, Y.; Kong, J. L.; Xiong, H. M. Biodegradable ZnO@Polymer Core-Shell Nanocarriers: pH-Triggered Release of Doxorubicin *in Vitro*. *Angew. Chem., Int. Ed.* **2013**, *52*, 4127–4131.

(28) Ye, D. X.; Ma, Y. Y.; Zhao, W.; Cao, H. M.; Kong, J. L.; Xiong, H. M.; Möhwald, H. ZnO-Based Nanoplatfoms for Labeling and Treatment of Mouse Tumors without Detectable Toxic Side Effects. *ACS Nano* **2016**, *10*, 4294–4300.

(29) Williams, H. C.; Dellavalle, R. P.; Garner, S. Acne Vulgaris. *The Lancet* **2012**, *379*, 361–372.

- (30) Zouboulis, C. C. Acne and Sebaceous Gland Function. *Clin. Dermatol.* **2004**, *22*, 360–366.
- (31) Zaenglein, A. L. Topical Retinoids in the Treatment of Acne Vulgaris. *Semin. Cutaneous Med. Surg.* **2008**, *27*, 177–182.
- (32) Huang, S.; Laoukili, J.; Epping, M. T.; Koster, J.; Holzel, M.; Westerman, B. A.; Nijkamp, W.; Hata, A.; Asgharzadeh, S.; Seeger, R. C.; Versteeg, R.; Beijersbergen, R. L.; Bernards, R. ZNF423 is Critically Required for Retinoic Acid-Induced Differentiation and is a Marker of Neuroblastoma Outcome. *Cancer Cell* **2009**, *15*, 328–340.
- (33) Matthay, K. K.; Reynolds, C. P.; Seeger, R. C.; Shimada, H.; Adkins, E. S.; Haas-Kogan, D.; Gerbing, R. B.; London, W. B.; Villablanca, J. G. Long-Term Results for Children with High-Risk Neuroblastoma Treated on a Randomized Trial of Myeloablative Therapy Followed by 13-Cis-Retinoic Acid: a Children's Oncology Group Study. *J. Clin. Oncol.* **2009**, *27*, 1007–1013.
- (34) Khan, A. W.; Kotta, S.; Ansari, S. H.; Sharma, R. K.; et al. Potentials and Challenges in Self-Nanoemulsifying Drug Delivery Systems. *Expert Opin. Drug Delivery* **2012**, *9*, 1305–1317.
- (35) Liu, J.; Hu, W.; Chen, H.; Ni, Q.; Xu, H.; Yang, X. Isotretinoin-Loaded Solid Lipid Nanoparticles with Skin Targeting for Topical Delivery. *Int. J. Pharm.* **2007**, *328*, 191–195.
- (36) Shah, K. A.; Date, A. A.; Joshi, M. D.; Patravale, V. B. Solid Lipid Nanoparticles (SLN) of Tretinoin: Potential in Topical Delivery. *Int. J. Pharm.* **2007**, *345*, 163–171.
- (37) Raza, K.; Singh, B.; Singla, S.; Wadhwa, S.; Garg, B.; Chhibber, S.; Katare, O. P. Nanocolloidal Carriers of Isotretinoin: Antimicrobial Activity Against Propionibacterium Acnes and Dermatokinetic Modeling. *Mol. Pharmaceutics* **2013**, *10*, 1958–1963.
- (38) Das, S.; Ng, W. K.; Tan, R. B. H. Are Nanostructured Lipid Carriers (Nlcs) Better than Solid Lipid Nanoparticles (Slns): Development, Characterizations and Comparative Evaluations of Clotrimazole-Loaded Slns and Nlcs? *Eur. J. Pharm. Sci.* **2012**, *47*, 139–151.
- (39) Xie, C.; Zhen, X.; Lei, Q.; Ni, R.; Pu, K. Self-Assembly of Semiconducting Polymer Amphiphiles for *in Vivo* Photoacoustic Imaging. *Adv. Funct. Mater.* **2017**, *27*, No. 1605397.
- (40) Lyu, Y.; Fang, Y.; Miao, Q.; Zhen, X.; Ding, D.; Pu, K. Intraparticle Molecular Orbital Engineering of Semiconducting Polymer Nanoparticles as Amplified Theranostics for *in Vivo* Photoacoustic Imaging and Photothermal Therapy. *ACS Nano* **2016**, *10*, 4472–4481.
- (41) Xie, C.; Upputuri, P. K.; Zhen, X.; Pramanik, M.; Pu, K. Self-Quenched Semiconducting Polymer Nanoparticles for Amplified *in Vivo* Photoacoustic Imaging. *Biomaterials* **2017**, *119*, 1–8.
- (42) Miao, Q. Q.; Lyu, Y.; Ding, D.; Pu, K. Y. Semiconducting Oligomer Nanoparticles as an Activatable Photoacoustic Probe with Amplified Brightness for *in Vivo* Imaging of pH. *Adv. Mater.* **2016**, *28*, 3662–3668.
- (43) Xiong, H. M.; Xu, Y.; Ren, Q. G.; Xia, Y. Y. Stable Aqueous ZnO@Polymer Core-Shell Nanoparticles with Tunable Photoluminescence and Their Application in Cell Imaging. *J. Am. Chem. Soc.* **2008**, *130*, 7522–7523.
- (44) Xiong, H. M.; Zhao, X.; Chen, J. S. New Polymer-Inorganic Nanocomposites: PEO-ZnO and PEO-ZnO-LiClO<sub>4</sub> Films. *J. Phys. Chem. B* **2001**, *105*, 10169–10174.
- (45) Bushue, N.; Wan, Y. J. Retinoid Pathway and Cancer Therapeutics. *Adv. Drug Delivery Rev.* **2010**, *62*, 1285–1298.
- (46) Pan, Z. Y.; Liang, J.; Zheng, Z. Z.; Wang, H. H.; Xiong, H. M. The Application of ZnO Luminescent Nanoparticles in Labeling Mice. *Contrast Media Mol. Imaging* **2011**, *6*, 328–330.
- (47) Roth, G. J.; Binder, R.; Colbatzky, F.; Dallinger, C.; Schlenker-Herceg, R.; Hilberg, F.; Wollin, S. L.; Kaiser, R. Nintedanib: from Discovery to the Clinic. *J. Med. Chem.* **2015**, *58*, 1053–1063.
- (48) Solomon, B. J.; Mok, T.; Kim, D. W.; Wu, Y. L.; Nakagawa, K.; Mekhail, T.; Felip, E.; Cappuzzo, F.; Paolini, J.; Usari, T.; Iyer, S.; Reisman, A.; Wilner, K. D.; Tursi, J.; Blackhall, F.; The PROFILE 1014 Investigators. First-Line Crizotinib Versus Chemotherapy in ALK-Positive Lung Cancer. *N. Engl. J. Med.* **2014**, *371*, 2167–2177.
- (49) Wang, Y.; Zhang, G.; Hu, G.; Bu, Y.; Lei, H.; Zuo, D.; Han, M.; Zhai, X.; Gong, P. Design, Synthesis and Biological Evaluation of Novel 4-Arylamino-pyrimidine Derivatives Possessing a Hydrazone Moiety as Dual Inhibitors of L1196M ALK and ROS1. *Eur. J. Med. Chem.* **2016**, *123*, 80–89.
- (50) Epstein Shochet, G.; Israeli-Shani, L.; Koslow, M.; Shitrit, D. Nintedanib (BIBF 1120) Blocks the Tumor Promoting Signals of Lung Fibroblast Soluble Microenvironment. *Lung Cancer* **2016**, *96*, 7–14.
- (51) Xiang, J. N.; Jiang, L. H.; Chen, C. Y.; Fu, Z. Y.; Duan, J. F.; He, X. X.; Wang, K. M. Studies on the Synthesis and Antiproliferative Activities of 13-Cis-Retinoyl Sugar Derivatives. *J. Carbohydr. Chem.* **2006**, *25*, 595–614.
- (52) Petkovich, M.; Brand, N. J.; et al. A Human Retinoic Acid Receptor which Belongs to the Family of Nuclear Receptors. *Nature* **1987**, *330*, 444–450.
- (53) Dollé, P. Developmental Expression of Retinoic Acid Receptors (Rars). *Nucl. Recept. Signaling* **2009**, *7*, No. e006.
- (54) Connolly, R. M.; Nguyen, N. K.; Sukumar, S. Molecular Pathways: Current Role and Future Directions of the Retinoic Acid Pathway in Cancer Prevention and Treatment. *Clin. Cancer Res.* **2013**, *19*, 1651–1659.
- (55) Theodosiou, M.; Laudet, V.; Schubert, M. From Carrot to Clinic: an Overview of the Retinoic Acid Signaling Pathway. *Cell. Mol. Life Sci.* **2010**, *67*, 1423–1445.